AGU ADVANCING EARTH AND SPACE SCIENCES

JGR Earth Surface

RESEARCH ARTICLE
10.1029/2024JF007831

# Segregation-Induced Flow Transitions in Rock-Ice Mixtures: Implications for Rock-Ice Avalanche Dynamics

**Gordon G. D. Zhou**[1,2,3], **Kahlil F. E. Cui**[1,2], **Lu Jing**[4], **Anne Mangeney**[5], **Yifei Cui**[6], **Yu Huang**[7], **and Xiaoqing Chen**[1,2,3]

[1]Key Laboratory of Mountain Hazards and Engineering Resiliences, Institute of Mountain Hazards and Environment, Chinese Academy of Sciences, Chengdu, China, [2]University of Chinese Academy of Sciences, Beijing, China, [3]China-Pakistan Joint Research Center on Earth Sciences, CAS-HEC, Chengdu, China, [4]Shenzhen International Graduate School, Institute for Ocean Engineering, Tsinghua University, Shenzhen, China, [5]Institut de Physique du Globe de Paris, Université Paris Cité, CNRS (UMR 7154), Paris, France, [6]State Key Laboratory of Hydroscience and Engineering, Tsinghua University, Beijing, China, [7]Department of Geotechnical Engineering, College of Civil Engineering, Tongji University, Shanghai, China

**Key Points:**

- Vertical segregation coupled with large friction differences results in sharp transitions in the flow profiles of rock-ice avalanches
- The rheology of rock-ice mixtures is governed by the interparticle contact probabilities
- Sharply varying flow profiles are modeled using the granular fluidity model incorporating the dependence on contact probabilities

**Supporting Information:**

Supporting Information may be found in the online version of this article.

**Correspondence to:**

G. G. D. Zhou and K. F. E. Cui,
gordon@imde.ac.cn;
kfcui@imde.ac.cn

**Citation:**

Zhou, G. G. D., Cui, K. F. E., Jing, L., Mangeney, A., Cui, Y., Huang, Y., & Chen, X. (2024). Segregation-induced flow transitions in rock-ice mixtures: Implications for rock-ice avalanche dynamics. *Journal of Geophysical Research: Earth Surface*, *129*, e2024JF007831. https://doi.org/10.1029/2024JF007831

Received 10 MAY 2024
Accepted 9 SEP 2024
Corrected 25 JAN 2025

This article was corrected on 25 JAN 2025. See the end of the full text for details.

**Author Contributions:**

**Conceptualization:** Gordon G. D. Zhou, Kahlil F. E. Cui, Lu Jing
**Formal analysis:** Gordon G. D. Zhou, Kahlil F. E. Cui, Lu Jing, Anne Mangeney
**Funding acquisition:** Gordon G. D. Zhou, Kahlil F. E. Cui
**Investigation:** Kahlil F. E. Cui
**Supervision:** Gordon G. D. Zhou, Lu Jing
**Writing – original draft:** Kahlil F. E. Cui
**Writing – review & editing:** Anne Mangeney, Yifei Cui, Yu Huang, Xiaoqing Chen



## Abstract

Global climate change has been intensifying the scale and frequency of rock-ice avalanches and similar catastrophic mass movements in high-mountain regions. The difference in the physical characteristics of rock and ice particles leads to mixing and segregation during flow. Although, both particle segregation and the presence of ice fundamentally alter flow behavior, the joint influence and feedback of these two aspects are overlooked in state-of-the-art rock-ice avalanche models. Using discrete element simulations, we show that by controlling the distribution of inter-particle frictional interactions within the mixture, segregation patterns resulting from the size, density, concentration, and surface friction differences of rock and ice phases can induce sharp velocity gradients along the flowing thickness. Flowing layers where low friction contacts with ice are abundant tend to flow faster and can induce slow creeping motion in an otherwise static basal layer dominated by more frictional rocks. Based on these observations, we find that the effective friction of rock-ice flows for various mixture concentrations and size ratios can be obtained as a sum of the single-phase rheologies of rocks and ice weighted according to their microscopic contact probabilities. This effective friction for rock-ice mixtures allows us to extend a recent non-local granular fluidity framework that captures the complex segregation-flow feedback mechanism in rock-ice flows. The findings provide a deeper micromechanical understanding of how particle interactions influence rock-ice avalanche mobility, which ultimately improves flow models needed for hazard assessment and mitigation.

## Plain Language Summary

Rock-ice avalanches are hazardous mass flows in alpine regions. Being granular in nature, the difference in the size, concentration, density, and surface roughness of rock and ice particles can drive them to segregate. However, the segregation of rocks and ice and its impacts on the bulk flow dynamics are overlooked in current rock-ice avalanche models. Using granular flow simulations, we show that size and density segregation, coupled with the surface friction difference between the rocks and ice, can induce sharp transitions in the avalanche flow velocity by controlling the probabilities in which rocks and ice contact with each other. This study highlights the importance of microscopic frictional interactions in modeling the flow resistance of rock-ice mixtures, and the enhanced understanding presented here may further improve rock-ice avalanche modeling necessary for hazard management.

## 1. Introduction

Rising mean annual temperatures (Huggel et al., 2010; Noetzli et al., 2006) and extreme weather conditions (Kääb et al., 2021) related to global climate change have increased the frequency of large slope failures in high-mountain regions (Deline et al., 2021; Huggel et al., 2010), exposing alpine communities and infrastructure to the risk of rock-ice avalanches. The historically devastating rock-ice avalanches in Nevado Huascaran, Peru (1962 and 1970) (Evans, Bishop, et al., 2009), in Kolka-Karmadon, Russian Caucasus (2002) (Evans, Tutubalina, et al., 2009), among others (Schneider, Huggel, et al., 2011; Sosio et al., 2012) have resulted in an accumulated death toll of more than 7,000 people (Evans, Bishop, et al., 2009) and the destruction of infrastructure located several kilometers away from the source. Recent massive rock-ice avalanches, including the $2.7 \times 10^7$ m$^3$ event in Chamoli, Uttarakhand, India (2021) that killed ~200 people and severely damaged two hydropower installations

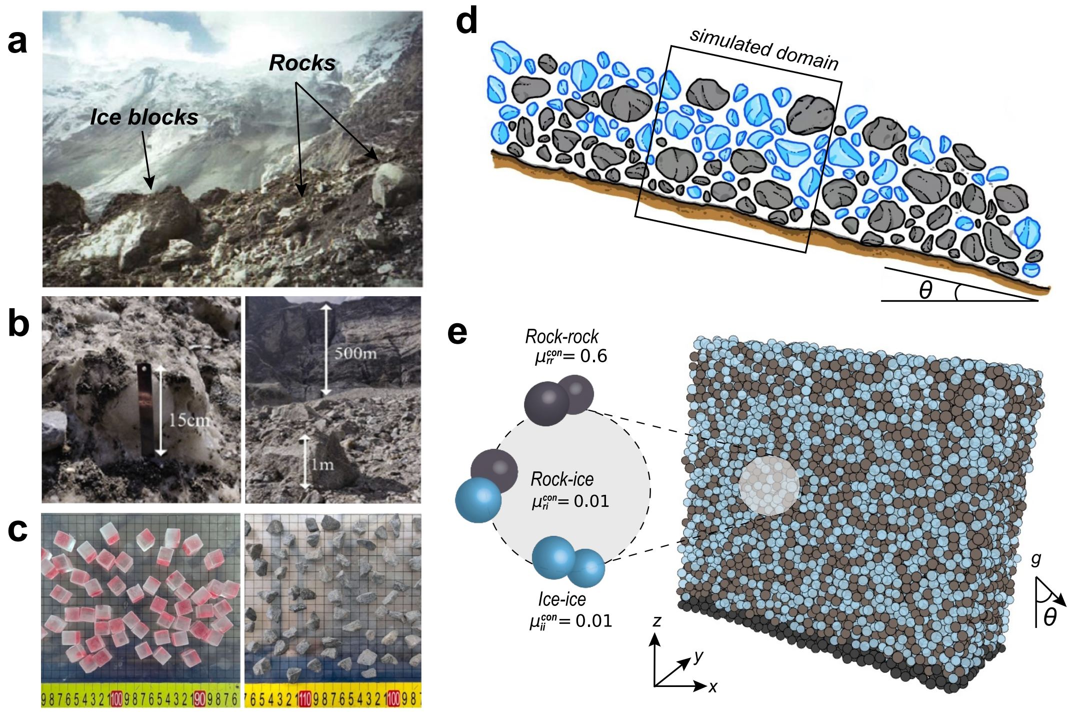


**Figure 1.** (a) Granular rocks and ice observed at the surface of Kolka glacier, Russian Caucasus prior to its collapse in 2002 (Haeberli et al., 2015), and in the (b) 2015 Langtang avalanche deposits (Gnyawali et al., 2020). (c) Gravel and ice particles used in rock-ice flow experiments; scale is in centimeters (Zhu et al., 2024) (d) Schematic diagram showing rock-ice avalanches as granular flows. (e) Snapshot of periodic flow of rock (brown) and ice (blue) particles and the coordinate plane. The magnified section highlights the three types of particle interactions within the mixture—rock-rock, rock-ice, and ice-ice—along with their contact friction coefficients.

(Shugar et al., 2021), have sparked increased interest in the research of rock-ice avalanche dynamics and in the development of effective numerical models for hazard mitigation (Favreau et al., 2010; Mergili et al., 2020; Moretti et al., 2012).

A rock-ice avalanche is distinguished from other mass flows due to the complex interactions between rock and ice particles, a major source of internal heterogeneity (Feng et al., 2023) and often unexpected mobility of the flow (Moretti et al., 2012). At least two mechanisms of the flow heterogeneity of rock-ice avalanches remain poorly explored, namely, granular segregation and its feedback effects on the flow rheology (Feng et al., 2023). In real rock-ice avalanches and in small-scale physical models, rock and ice phases can exist as particulate matter (Figures 1a–1c) (Gnyawali et al., 2020; Haeberli et al., 2015), where granular phenomena such as particle segregation are significant (Gray & Ancey, 2015). Differences in the size, density, and surface friction of ice and rock drive them to segregate and form stratified layers along the flow thickness (Zhu et al., 2024). Shearing during flow partially melts the ice, creating a layer of meltwater that reduces its surface friction (Turnbull, 2011), leading to decreased bulk flow resistance and improved flowability (Schneider, Kaitna, et al., 2011). The continuous shearing of the ice phase also provides a constant supply of meltwater, which fluidizes the avalanche (Pudasaini & Krautblatter, 2014; Schneider, Kaitna, et al., 2011). It is reasonable to expect that flowing layers rich in less frictional ice particles will flow faster compared to layers dominated by or mixed with rocks. For example, depth-averaged models for rock-ice avalanches require smaller effective friction coefficients to reproduce their dynamics and runout than when simulating rock avalanches (Moretti et al., 2012), although it may be difficult to discern if the reduced effective friction is due to rock-ice frictional properties or basal slipping over a glacier (Moretti et al., 2012, 2015). Particle segregation impacts granular flow mobility (Barker et al., 2021) and in rock-ice avalanches, the stratified flow layers may result in more complex flow behaviors that are not currently considered in state-of-the-art numerical models (Pudasaini & Krautblatter, 2014; Sansone et al., 2021).

Here we reveal how the segregation of rock and ice particles along the vertical direction can result in highly heterogeneous flow profiles in rock-ice avalanches. Due to the sparseness of real-world data of rock-ice avalanches (Deline et al., 2014; Schneider, Huggel, et al., 2011; Sosio, 2015), we use discrete element method (DEM) simulations of spherical particles that are different in size, density, and surface friction to systematically study the segregation and rheology of rock-ice mixtures in a gravity-driven granular flow configuration, a common simplification of complex geophysical flows (Delannay et al., 2017). We find various inertial and creeping flow regimes depending on the state of mixing and segregation, which, from a microscopic perspective, are governed by the contact probabilities of the two particle species. The flow profiles in different flow regimes can be modeled by extending a recently established non-local granular fluidity framework by incorporating information of microscopic frictional contact probabilities. Moreover, as we focus on the fundamental role of particle interactions, we only consider situations where meltwater merely wets the surface of the ice particles (Schneider, Kaitna, et al., 2011). Additional complexities such as fluidization from excess meltwater generation (Mergili et al., 2020; Shugar et al., 2021) and flow over glaciers (Favreau et al., 2010; Moretti et al., 2012) will be considered in future work.

## 2. Methodology

### 2.1. Discrete Element Method Modeling of Rock-Ice Avalanches

Rock-ice avalanches are simulated using DEM as a mixture of inelastic rock and ice particles flowing down a rough incline at an angle $\theta$ (Figure 1d). The Hertz contact model is used to simulate particle interactions. The governing equations for the DEM are detailed in Appendix A. The 0.175 m long, 0.1 m wide, 0.15 m thick computational domain is periodic along the streamwise ($x$-direction) and spanwise ($y$-direction) directions to simulate a very long and wide flow (Figure 1e; see also Figures 3c–3f), consistent with the depth-averaged assumption typically adopted in landslide or avalanche modeling. The base is roughened by installing a randomly arranged layer of immobile particles.

Ice and rock particles have distinct material and contact properties. Rock particles are assigned a density of 2,500 kg/m$^3$, Poisson's ratio of 0.3, and a restitution coefficient of 0.8 based on the properties of rocks observed in natural rock-ice avalanches (Sosio et al., 2012) and experiments (Schneider, Huggel, et al., 2011; Schneider, Kaitna, et al., 2011; Yang et al., 2019). To facilitate efficient simulations, a lower Young's Modulus of 50 MPa is used (two orders of magnitude lower than that of real rocks), although this reduction has been shown to have minimal effect on segregation (Jing et al., 2017) and on steady granular flows (Silbert et al., 2001). The ice particles have a Poisson's ratio of 0.3 (Gold, 1977) and are assigned a density of 1,000 kg/m$^3$, which is slightly higher than that of real ice which is 917 kg/m$^3$ although this difference does not influence the conclusions of this work. Similar to the rocks, the Young's modulus of ice (Gammon et al., 1983; Gold, 1977) is scaled down by two orders of magnitude, 10 MPa. The restitution coefficients of rock and ice are the same (Higa et al., 1996).

Since the material properties of ice change with its temperature (Higa et al., 1996), important simplifying assumptions on its material and contact properties are adopted here based on the literature. (a) The flow internal temperature is assumed to remain constantly low (≤0°C) in which case material properties do not significantly change. Thermal interactions are not included in the modeling. (b) Meltwater only reduces the interparticle friction of ice. Cohesion due to meltwater is not modeled following experimental observations that ice mainly improves the flow, indicating that meltwater lubrication dominates cohesive effects (Schneider, Kaitna, et al., 2011; Sosio et al., 2012). (c) Real ice and rocks are angular or irregularly shaped (Schneider, Kaitna, et al., 2011), however simulated particles are made spherical and unbreakable to highlight the impacts of size, density, and surface friction differences on the segregation and mixture rheology. These conditions generally apply to the 'dry stage' in the rotating drum experiments of Schneider, Kaitna, et al. (2011) and are the prevalent conditions during the early stages of rock ice avalanches (Mergili et al., 2020). Ice in rock-ice avalanches do not only exist as granules but can be wedged between the rock matrix binding them together (Pouragha et al., 2023). Our simulations do not consider interstitial ice since they are not directly involved in the frictional-collisional interactions during flow.

Since all particles are uniformly shaped, the friction that prevents contacting particles from sliding against each other is only due to microscopic surface irregularities quantified by the interparticle friction coefficient. The coefficients of friction at rock-rock, ice-ice, and rock-ice contacts are denoted as $\mu_{rr}^{\mathrm{con}}$, $\mu_{ii}^{\mathrm{con}}$, and $\mu_{ri}^{\mathrm{con}}$, respectively. Although more frictional interactions may exist in real rock-ice avalanches due to the wide range of particle types, we focus only on three fundamental interactions due to the great distinction of the material properties of ice and

10.1029/2024JF007831

rock. Based on previous DEM simulations of rock-type materials (Shen et al., 2020; T. Zhao & Liu, 2020), $\mu_{rr}^{con}$ is set to be 0.6. We model the effect of surface meltwater wetting by using a very small contact friction for both ice-ice and rock-ice contacts $\mu_{ii}^{\mathrm{con}} = \mu_{ri}^{\mathrm{con}} = 0.01$ (Jones et al., 1994; Ren et al., 2021; G. Wang & Calvetti, 2021). Setting these friction coefficients equal is a simplification that allows easier evaluation of the role of frictional interactions in rock-ice flows although general scenarios where they are dissimilar are also investigated here. Basal particles are assigned similar contact properties to rocks.

Different mixtures are simulated by varying the diameter ratio of the rock over the ice particles, $R = d_r/d_i \in [0.5, 2]$, and the volumetric ice concentration, $\overline{C}_i \in [0.2, 0.8]$. The small particle diameter is held constant at a mean value of 0.005 m and $R$ is varied by increasing the large particle diameter. A slight polydispersity of 10% is applied to both particle sizes to prevent geometric ordering. The number of simulated particles is sufficient to ensure that the simulation results are roughly independent of it (see Figure S1 in Supporting Information S1). Rock-ice avalanches are initiated from the collapse of glaciers or steep ice-laden mountain slopes (Haeberli et al., 2015; Shugar et al., 2021) but may also occur at gentler inclinations (Kääb et al., 2021). Prior to collapse, slabs of ice cover bed rock or moraines or are meshed in between the rock matrix. Since we are only interested in the steady flow behavior, long after the initial collapse and the disintegration of the larger blocks of rock and ice, we do not mimic real initiation scenarios and particles are initiated from rest by tilting the $xy$ plane to a designated $\theta$. To consistently study segregation dynamics in different mixture scenarios, all cases are initially well-mixed. Steady, fully developed flows of pure ice particles $\left(\overline{C}_i = 1\right)$ are obtained at $9° \le \theta \le 23°$, while the more frictional rock particles $\left(\overline{C}_i = 0\right)$ need a range of greater inclination angles ($21° \le \theta \le 35°$). Particles do not flow below the minimum flow angles, while above the maximum flow angles particles are already accelerating. Rock-ice mixtures are simulated over $12° \le \theta \le 23°$ involving slopes below the minimum $\theta$ of rocks (21°) and below the maximum $\theta$ of ice (23°). Note that ice-laden mountain faces and glaciers can remain stable above the simulated inclinations. The angles used here only reflect the range of steepness in which dense flows of spherical particles with material properties similar to those of rock and ice are possible.

### 2.2. Comparing Simulations With Natural and Experimental Rock-Ice Avalanches

We compare the depth-averaged results of our simulations with previous experiments (Dong & Su, 2024; Schneider, Kaitna, et al., 2011; C. Wang et al., 2022) and field data of 34 natural rock-ice avalanches derived from the literature. Dynamic similarity is assessed using the Bagnold number $N_{\mathrm{Bag}} = \frac{\phi\overline{\rho}\overline{d}^2\dot{\gamma}}{(1-\phi)\eta_F}$, which quantifies the relative significance of inter-granular collisional stresses over viscous stresses, and the Savage number $N_{\mathrm{Sav}} = \frac{\overline{\rho}\overline{d}^2\dot{\gamma}^2}{(\overline{\rho}-\rho_F)gH}$ which is the ratio of collisional over frictional stresses. $\phi$ is the solid volume fraction, $\overline{\rho}$ is the solid density, $\eta_F$ and $\rho_F$ are the pore fluid viscosity and density, and $g$ is the gravity acceleration. Depending on available data, the shear rate $\dot{\gamma}$ for the field cases is calculated using either the maximum or mean flow velocities and thicknesses $H$. The mean particle diameter $\overline{d}$ is rarely documented for the field cases, hence we use the small particle diameter in the simulations (0.005 m) to calculate $N_{\mathrm{Bag}}$ and $N_{\mathrm{Sav}}$. We discriminate the dry from saturated (as indicated in the literature) experiments and field cases. Calculation details for experiments and field cases are detailed in the Data Set S1.

Figure 2b shows that data points for our simulations and the dry experiments collapse along a single power-law curve $N_{\mathrm{Bag}} = \alpha N_{\mathrm{Sav}}^{\beta}$, where $\alpha$ and $\beta$ are fitting coefficients, suggesting that they may be in a similar flow regime. Field case data scale similarly with the simulations and experiments (similar $\beta$ value), but are shifted upwards despite using a small particle diameter. This is possibly related to the much greater flowing thicknesses (and volumes) of the natural flows (Schneider, Kaitna, et al., 2011). Meanwhile, saturated rock-ice flows shift downward with increased influence of viscous stresses on flow dynamics. Using a larger mean grain size for the dry and saturated field cases shifts the best-fit curves upward (see Figure S2 in Supporting Information S1). The dynamic similarity of the simulations with the experimental avalanches, and their closeness to those of the dry field cases, suggests that to some extent our idealized modeling captures the dynamics of real rock-ice flows.

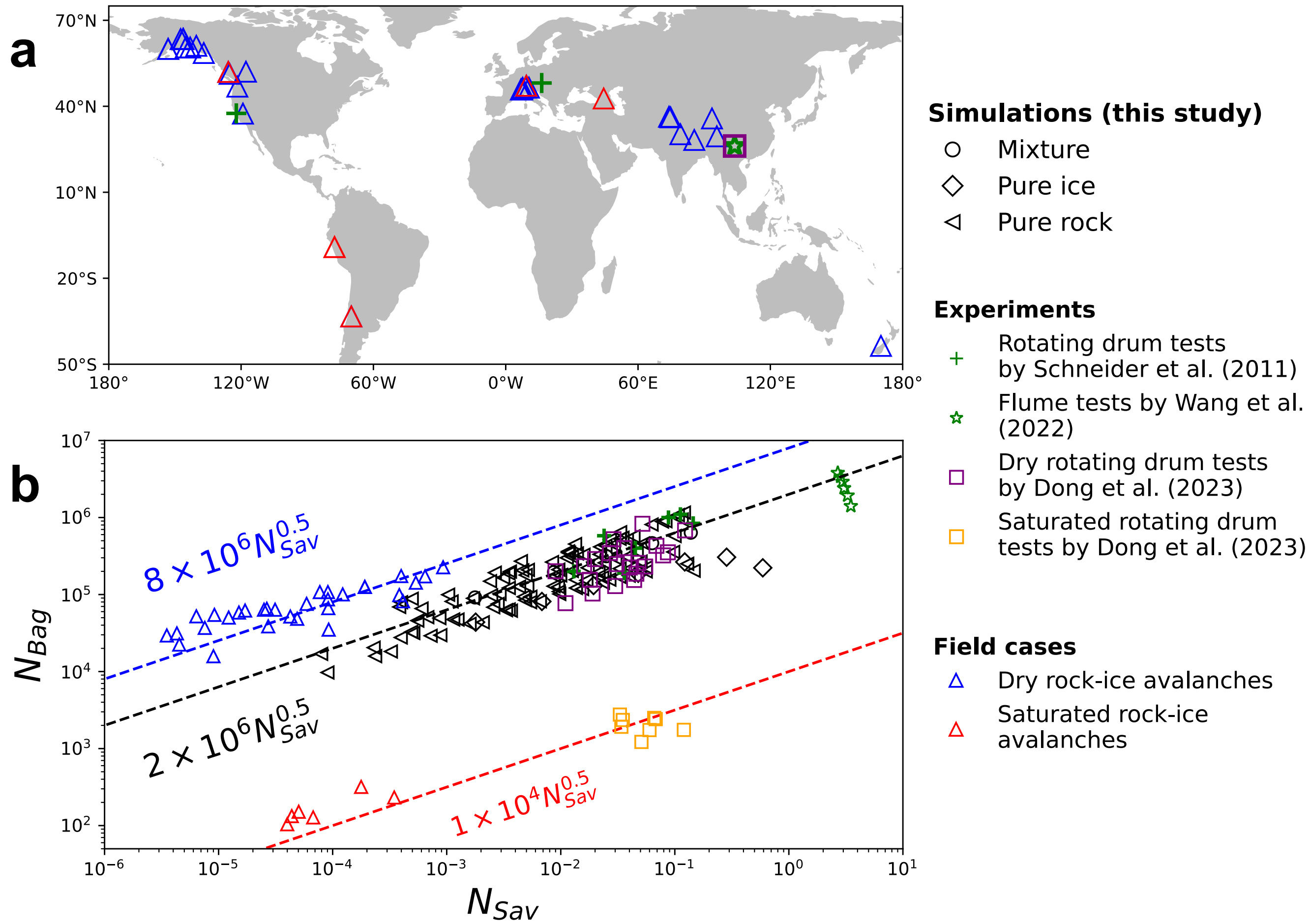


**Figure 2.** (a) Global distribution of selected rock-ice avalanches and experiments. (b) Comparing the mobility of simulated, experimental, and natural rock-ice avalanches through the Savage $N_{\mathrm{Sav}}$ and Bagnold $N_{\mathrm{Bag}}$ numbers.

## 3. Results

### 3.1. Segregation Patterns Induce Transitions in Flow Profiles

In our simulations, segregation inevitably occurs due to the difference in the particle size and density of rock and ice particles. Figure 3a shows the vertical trajectory of the ice and rock particles' centers of mass, $\mathrm{COM}_i$ and $\mathrm{COM}_r$, respectively, in dimensionless time $t/\sqrt{H/g}$. For the example case $R = 1, \overline{C}_i = 0.5, \theta = 20°$ the ice (rock) phase moves up (down), eventually reaching a steady level. The time at which the rising particle specie reaches 90% of its steady height is labeled $t_{\mathrm{seg}}$. The inset plot shows that segregation is typically completed after $t_{\mathrm{seg}} \sim 250$. Real rock-ice avalanches have greater flow thicknesses and segregation may still be incomplete upon termination. For example, using the mean $t_{\mathrm{seg}}$, segregation in the 2005 Mt. Steller avalanche (Moretti et al., 2012; Sosio et al., 2012), having mean flow thicknesses of 10–15 m, would be completed in 252–309 s which is much longer than its flowing time of 130 s. This is probably the reason why segregation in rock-ice avalanches is very seldom observed in deposits, coupled with the fact that most of the ice melts during the course of the flow due to continuous shear. Nevertheless, as will be shown below, studying idealized segregation scenarios allows us to reveal a general dependence of the flow rheology on the rock and ice concentration.

The thickness of the segregated layers depends on the cooperation and competition of size and density segregation mechanisms (Duan et al., 2021). Density segregation is a buoyancy-driven process where heavier particles "sink" downward while lighter particles rise to the free surface. Size segregation, drives larger particles to the top through persistent frictional interactions with neighboring particles, while smaller particles percolate downwards under gravity through shear-generated voids (Gray, 2018). We quantify the degree of steady-state segregation as

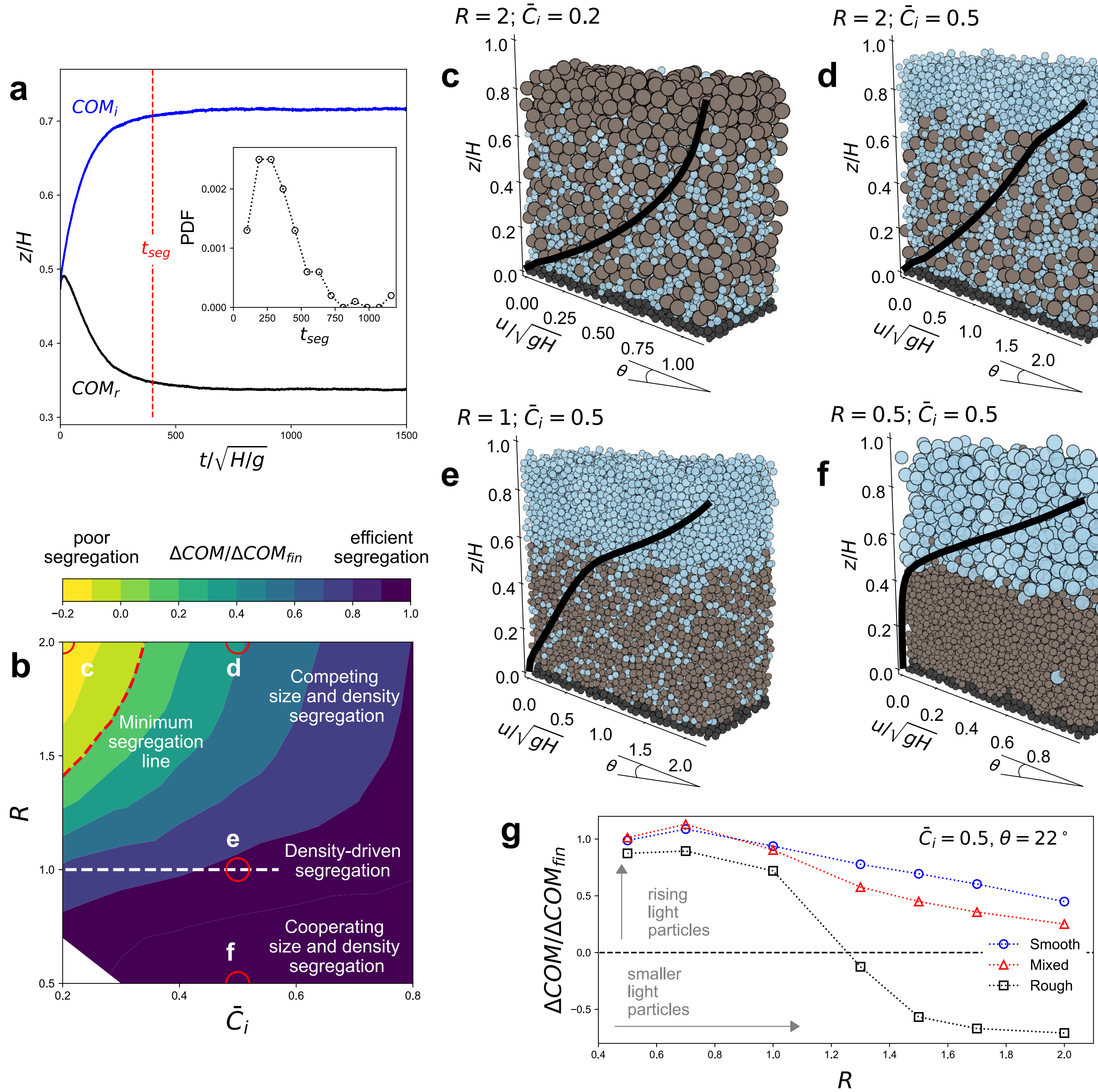


**Figure 3.** Segregation in rock-ice avalanches. (a) Trajectory of ice (blue) and rock (black) particles during segregation for a $R = 1$, $\overline{C}_i = 0.5, \theta = 20°$ mixture. Red line indicates $t_{seg}$. Inset plot shows the probability distribution of $t_{seg}$ for all simulations. (b) Degrees of segregation in the $R - \overline{C}_i$ parameter space at $\theta = 20°$. Red dashed line represents minimum $R$ and $\overline{C}_i$ necessary for segregation. (c–f) Snapshots of selected simulations after reaching steady state segregation, with the associated velocity profile plotted in the axes. (g) The segregation of rock-ice mixtures compared to size and density bidisperse mixtures having only rough and smooth contacts for different $R$ and $\overline{C}_i = 0.5$, $\theta = 22°$.

$\Delta COM/\Delta COM_{fin}$ where $\Delta COM = (COM_i - COM_r)$ and $\Delta COM_{fin}$ is the $\Delta COM$ for a hypothetical perfect-segregation scenario where all ice particles segregate to the top (Jing et al., 2017). By this definition, $\Delta COM/\Delta COM_{fin} = 1$ when all ice particles segregate upward, 0 when they are evenly mixed with the rocks, and −1 when they segregate downward. Plotting $\Delta COM/\Delta COM_{fin}$ in the $R - \overline{C}_i$ space for $\theta = 20°$ in Figure 3d, reveals three main segregation scenarios. The missing data point for $R = 0.5$, $\overline{C}_i = 0.2$ is because the mixture does not flow under these simulation conditions. Snapshots of cases representing these scenarios are shown in Figures 3c–3f.

In the $R > 1$ scenario, size and density segregation compete and result in $\Delta COM/\Delta COM_{fin} \ll 1$. The upward size-driven segregation of large but heavy rock particles is counterbalanced by their tendency to sink (Duan et al., 2021; Jing et al., 2020). Segregation is sensitive to $\overline{C}_i$ in this scenario and the red dashed curve in Figure 3b marks the minimum segregation limit which separates negative (yellowish zones) and positive (blueish zones) $\Delta\text{COM}/\Delta\text{COM}_{\text{fin}}$. When there is a greater concentration of large rock particles (e.g., $R = 2$, $\overline{C}_i = 0.2$; Figure 3c), ice particles constantly fall between interstices leading to negative $\Delta\text{COM}/\Delta\text{COM}_{\text{fin}}$ values. Increasing $\overline{C}_i$ allows a layer of ice to form at the free-surface (e.g., $R = 2$, $\overline{C}_i = 0.5$; Figure 3d), as more voids become occupied. In the second segregation scenario, $R = 1$, only density segregation drives the separation of the rock and ice (Figure 3e). Finally, when $R < 1$, size and density-driven segregation mechanisms cooperate, resulting in the efficient separation of large, light ice and small, heavy rock particles (Figure 3f), that is, $\Delta\text{COM}/\Delta\text{COM}_{\text{fin}} \approx 1$.

We investigate the influence of interparticle friction on segregation in Figure 3g, by comparing the $\Delta\text{COM}/\Delta\text{COM}_{\text{fin}}$ of rock-ice mixtures (red triangles) with size- and density-bidisperse mixtures with only smooth ($\mu^{\text{con}} = 0.01$, blue circles) and rough ($\mu^{\text{con}} = 0.6$, black squares) contacts across different $R$ while $\overline{C}_i = 0.5$ and $\theta = 22°$. In this comparison, $\Delta\text{COM}_{\text{fin}}$ is the hypothetical scenario where all the light particles rise upward. When $R \leq 1$, segregation is insensitive to the interparticle friction since both size and density segregation mechanisms cooperate resulting in $\Delta\text{COM}/\Delta\text{COM}_{\text{fin}} \sim 1$. When the segregation mechanisms compete ($R > 1$), interparticle friction becomes relevant. Since the upward segregation of large particles depends on enduring frictional contacts with their surroundings (Jing et al., 2017), their tendency to rise is weakened when all particles are smooth. Density segregation, on the other hand, is less affected and drives the small light particles upward. This mechanism also holds true for the rock-ice mixtures since at these size ratios, large rocks are mostly in contact with the less frictional ice particles (Figures 3e and 3f). In high $\mu^{\text{con}}$ flow size segregation can compete with density segregation, driving more of the large, dense particles upward. This shows that the difference in interparticle friction changes the relative magnitude of size and density-driven segregation mechanisms, thereby shifting the minimum segregation conditions ($\Delta\text{COM}/\Delta\text{COM}_{\text{fin}} = 0$, dashed line).

The super-imposed velocity profiles in Figures 3c–3f demonstrate a potential dependence of the rock-ice flow mobility on the segregation patterns. When rock and ice particles remain well-mixed (Figure 3e), a typical Bagnold-like velocity profile is observed. When segregation is significant (Figures 3d–3f), the mixture is split into an ice-rich region near the free-surface and a mixing region with lower ice concentration $C_i$. This sharp concentration gradient results in an abrupt change in the velocity profile, $u(z)$, where the ice-rich region flows faster than the lower mixing regions. Interestingly, since the flow is below the minimum $\theta$ for the simulated rock particles (Pouliquen, 1999), rock-rich flow layers become nearly stationary (Figure 3f) and are driven only to slow creeping motion by the more mobile ice-rich layer above.

### 3.2. Granular Rheology of Rock-Ice Mixtures Depends on the Contact Probabilities of Rock and Ice

Models for rock-ice flows need to incorporate the phase concentration dependence into an appropriate rheological law. Granular rheology for bidisperse gravity-driven flows can be evaluated from the relationship of $\mu = \tau/P$ and the inertial number $I = \dot{\gamma}\overline{d}\sqrt{\overline{\rho}/P}$ (Jop et al., 2006), where $\tau$ is shear stress and $P$ is pressure. To account for different species diameters and densities, we define the mixture diameter as $\overline{d} = C_i d_i + (1 - C_i)\, d_r$ and density as $\overline{\rho} = C_i\rho_i + (1 - C_i)\rho_r$ (Tripathi & Khakhar, 2011). Layer-wise rheological data are obtained along the flow depth from each simulation (calculation methods in Appendix A). To illustrate the basic rheological characteristics of ice and rock flows, we first plot $\mu$ versus $I$ curves for pure ice (blue crosses) and rock particles (black crosses) in Figure 4a, both of which can be modeled using the well-known $\mu^{\text{in}}(I)$ law for dense granular flows (Jop et al., 2006):

$$\mu^{\text{in}}_{i(r)}(I) = \mu_{1,i(r)} + \frac{\mu_{2,i(r)} - \mu_{1,i(r)}}{1 + I_{o,i(r)}/I} \tag{1}$$

The superscript in indicates "inertial flow," $\mu_{1,i(r)}$ and $\mu_{2,i(r)}$ are the lower and upper limiting friction coefficients, respectively, $I_{o,i(r)}$ is a fitting constant. Subscripts $i$ and $r$ denote that the coefficients are for the pure ice and rock flows, respectively. Values of these single-phase coefficients are summarized in Table 1. Figure 4a shows that $\mu^{\text{in}}_r(I)$ is higher than $\mu^{\text{in}}_i(I)$, which is mainly due to the difference in the particle contact-scale friction parameter (Man et al., 2023). Differences in material density and Young's modulus do not result in a great shift in the $\mu_i(I)$ curves (Tripathi & Khakhar, 2011). Mixture flow data points fall on and in-between the two single-phase flow curves, and span horizontally for each angle of inclination, that is, $\mu = \tan\theta$, as expected for steady, fully

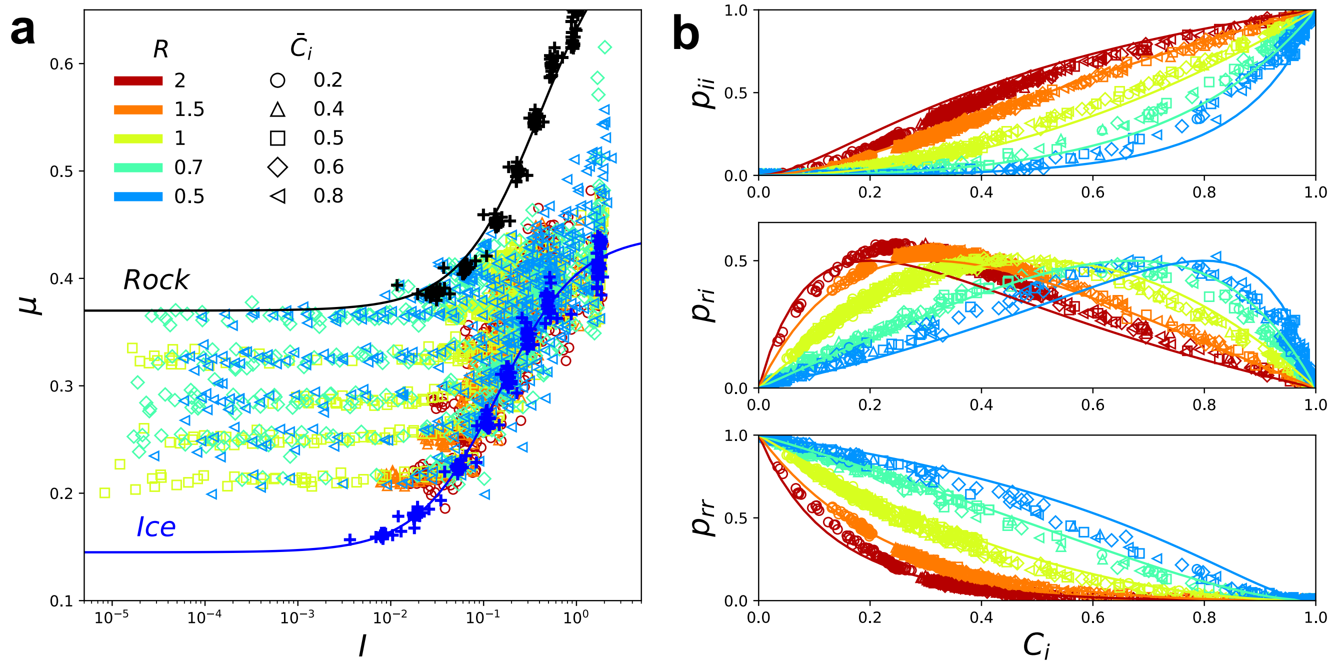


**Figure 4.** Granular rheology of rock-ice mixtures. (a) Data points for each flow layer projected in the $\mu$-$I$ space. Solid lines are the best-fits for Equation 1 for pure ice (blue) and rock (black) flows. (b) The change of the calculated (symbols) and theoretical (solid lines) $p_{rr}$, $p_{ii}$, $p_{ri}$ with $C_i$. Symbols and colors are similar to those in (a).

developed inclined flows due to momentum balance (Midi, 2004). The range of $\mu$ values obtained from the simulations are also in good agreement with those fitted on seismic data for rock-ice avalanches ($\mu = 0.19$) (Moretti et al., 2012).

The rock-ice mixture flows obviously depend on the frictional interactions among particle species. Flow layers dominated by smooth contacts between similar ice particles flow like pure ice with data falling along $\mu_i^{\text{in}}(I)$. Since $\mu_{ri}^{\text{con}} = \mu_{ii}^{\text{con}}$, flow layers rich in rock-ice contacts should also be close to $\mu_i^{\text{in}}(I)$. High-friction contacts between rock particles increase $\mu$, and data for flow layers dominated by rock particles approach $\mu_r^{\text{in}}(I)$. From this understanding, we hypothesize that the rheology of rock-ice mixtures depend on the distribution of frictional interactions within the granular flow. We propose that mixture rheology can be modeled as a sum of the single-phase $\mu^{\text{in}}(I)$ curves weighted according to the probability that the frictional interactions characterizing the single-phase flows occur within the mixture:

**Table 1**
*Best-Fit Frictional Coefficients for the $\mu^{in}(I)$ Rheology of Single-Phase Flows With Different Contact Frictions for Both Gravity-Driven and Plane Shear Simulations*

| Flow-type | $\mu^{\text{con}}$ | $\mu_1$ | $\mu_2$ | $I_0$ |
|---|---|---|---|---|
| Gravity-driven flows | 0.01 | 0.144 | 0.44 | 0.147 |
| | 0.05[a] | 0.21 | 0.548 | 0.289 |
| | 0.1[a] | 0.245 | 0.60 | 0.3 |
| | 0.6 | 0.38 | 0.74 | 0.412 |
| Planar-shear flows | 0.01 | 0.16 | 0.478 | 0.127 |
| | 0.05 | 0.21 | 0.548 | 0.289 |
| | 0.1 | 0.261 | 0.672 | 0.412 |
| | 0.6 | 0.38 | 0.74 | 0.427 |

[a]Used in Section 3.3.

$$
\begin{aligned}
\bar{\mu}_1 &= p_{ii}\mu_{1,i} + p_{rr}\mu_{1,r} + p_{ri}\mu_{1,ri} \\
\bar{\mu}_2 &= p_{ii}\mu_{2,i} + p_{rr}\mu_{2,r} + p_{ri}\mu_{2,ri} \\
\bar{I}_o &= p_{ii}I_{0,i} + p_{rr}I_{0,r} + p_{ri}I_{0,ri}
\end{aligned} \tag{2}
$$

The contact probabilities of ice on ice $p_{ii}$, rock on rock $p_{rr}$, and rock on ice $p_{ri}$ are calculated as (Jiang et al., 2023; Man et al., 2022):

$$
\begin{aligned}
p_{ii} &= (p_i)^2 \\
p_{rr} &= (p_r)^2 \\
p_{ri} &= 1 - p_{ii} - p_{rr}
\end{aligned} \tag{3}
$$

where $p_i$ and $p_r$ are the probabilities of finding rock and ice particles around a particle surface, respectively. Figure 4b shows that the relationship of the calculated $p_{ii}$, $p_{rr}$, and $p_{ri}$ (the fraction of specific particle contacts over the total number of contacts at a flow height) with $C_i$ varies with $R$ but not with $\theta$

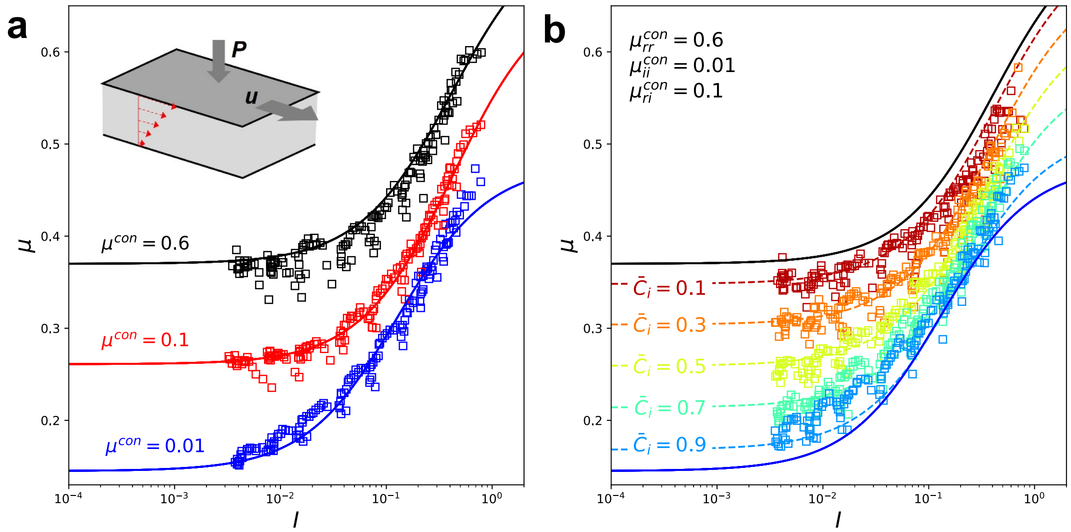


**Figure 5.** (a) The single-phase rheology of particles with $\mu^{\text{con}} = 0.01$ (black), $\mu^{\text{con}} = 0.1$ (red), and $\mu^{\text{con}} = 0.6$ (blue). The inset plot shows the schematic diagram of the simulated flow. (b) Planar shear flow simulations of mixtures where $\mu_{ri}^{\text{con}} = 0.1$, $\mu_{ii}^{\text{con}} = 0.01$, $\mu_{rr}^{\text{con}} = 0.6$ for different $\overline{C}_i$. Dashed lines are predictions made using equation (2–5), solid lines are best-fits for $\mu^{\text{con}} = 0.01$ (blue), and $\mu^{\text{con}} = 0.6$ (black).

(hence $\dot{\gamma}$) nor $\overline{C}_i$. The dependence of the contact probability on the particle type and size can be expressed as (Jiang et al., 2023):

$$p_{L(S)} = n_{L(S)} d_{L(S)} / (n_L d_L + n_S d_S) \tag{4}$$

Subscripts $L$ and $S$ denote large and small particle sizes where $r = L$ and $i = S$ when $R \geq 1$, while the opposite is true when $R < 1$. $n_L$ and $n_S$ are the number of large and small particles, respectively, and are related as (Jiang et al., 2023):

$$\frac{n_L}{n_S} = \frac{C_L C_S}{(d_L/d_S)^3} \tag{5}$$

The model requires the layer-wise size species concentration $C_{L(S)}$ as input, which can be predicted from existing size and density segregation equations (Duan et al., 2021; Gray & Ancey, 2015; Tunuguntla et al., 2014), although these models need to be modified to incorporate the influence of interparticle friction differences. Figure 4b shows that the contact probabilities predicted using Equations 3–5 show good correspondence with the DEM data.

Testing Equations 2–5 on our inclined flow simulations is not straightforward since the data spans horizontally, and does not clearly reflect the dependence on the mixture concentration. To better demonstrate the dependence of mixture rheology on the frictional contact probability, we conduct planar shear flow simulations where particles, having the same mean diameters (0.005 m) and densities (2,500 kg/m$^3$), are sheared in a streamwise ($x$) and spanwise ($y$) periodic domain. In these simulations, we inhibit size and density segregation to better illustrate the effects of interparticle friction difference. The 0.15 m long, 0.05 m wide, and 0.15 m thick granular bed is confined by a lid that constantly pushes down at a constant pressure while at the same time translates along the streamwise direction at a constant velocity. The shear rate is varied between $\dot{\gamma} = [0.1,..,50]\, s^{-1}$ and the ice concentration is varied between $\overline{C}_i = [0.1,\ldots,0.9]$. A constant $\dot{\gamma}$ is maintained along the flow thickness by applying a small stabilizing force proportional to $\dot{\gamma}z - u(z)$ to each particle at a height $z$ with a streamwise velocity $u$ at each timestep (Fry et al., 2018). In the gravity-driven flow simulations, $\mu_{1,ri} = \mu_{1,i}$, $\mu_{2,ri} = \mu_{2,i}$, and $I_{o,ri} = I_{o,i}$, because we set $\mu_{ri}^{\text{con}} = \mu_{ii}^{\text{con}}$. In the planar shear flow simulations, we adopt a general mixture scenario $\left(\mu_{ri}^{\text{con}} = 0.1,\ \mu_{ii}^{\text{con}} = 0.01,\ \mu_{rr}^{\text{con}} = 0.6\right)$ where $\mu_{ri}^{\text{con}} \neq \mu_{ii}^{\text{con}}$, hence the resulting mixture rheology should be a combination of three single-phase rheologies. Figure 5a shows the rheology and best-fits of single-phase flows having $\mu^{\text{con}} = 0.6$ (black), $\mu^{\text{con}} = 0.1$ (red), and $\mu^{\text{con}} = 0.01$ (blue); best-fit coefficients are summarized in Table 1.

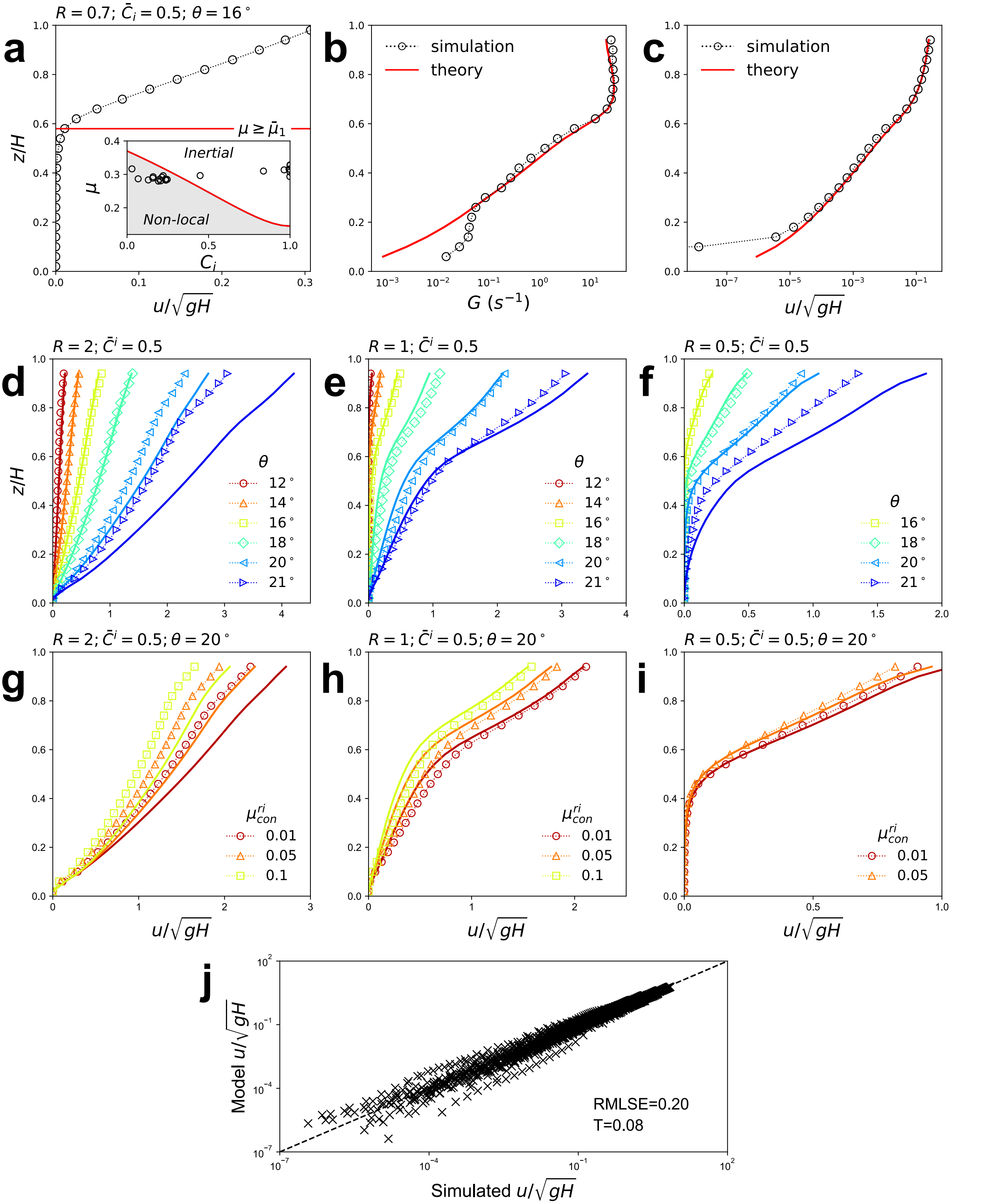

a
$R = 0.7; \bar{C}_i = 0.5; \theta = 16^\circ$
$\mu \geq \bar{\mu}_1$
Inertial
Non-local
$\mu$
$C_i$
z/H
$u/\sqrt{gH}$
b
simulation
theory
$G\ (s^{-1})$
c
simulation
theory
$u/\sqrt{gH}$
d
$R = 2; \bar{C}^i = 0.5$
$\theta$
12°
14°
16°
18°
20°
21°
e
$R = 1; \bar{C}^i = 0.5$
f
$R = 0.5; \bar{C}^i = 0.5$
g
$R = 2; \bar{C}^i = 0.5; \theta = 20^\circ$
$\mu^{ri}_{con}$
0.01
0.05
0.1
h
$R = 1; \bar{C}^i = 0.5; \theta = 20^\circ$
i
$R = 0.5; \bar{C}^i = 0.5; \theta = 20^\circ$
j
Model $u/\sqrt{gH}$
Simulated $u/\sqrt{gH}$
RMLSE=0.20
T=0.08


**Figure 6.**

Figure 5b shows the rheology of contact friction-different mixtures wherein increasing (decreasing) $\overline{C}_i$ clearly shifts the data downward (upward). By inputting the best-fit $\mu_i^{\mathrm{in}}(I)$ coefficients of single-phase flows into Equation 2 we obtain good predictions of the mixture rheology (dashed lines).

### 3.3. Modeling Segregation-Induced Flow Transitions

Figure 6a shows that in flows exhibiting creep flow ($\overline{C}_i = 0.5$, $R = 0.7$, $\theta = 16°$), $\mu < \overline{\mu}_1$ in some flow layers (see inset). The theoretical $\overline{\mu}_1(C_i)$ curve in the inset is obtained from Equation 2. Granular flows where $\mu \leq \mu_1$ are considered non-local flows where the stresses are no longer directly related to the shear rate through the $\mu^{\mathrm{in}}(I)$ rheology but instead on cooperative effects from neighboring particle layers (Henann & Kamrin, 2013). The height where $\mu \leq \overline{\mu}_1$ (red horizontal line) coincides with the transition toward creeping flow, showing that creeping is a non-local phenomenon and that the transition to creeping is controlled by the yield stress of the rock and ice mixture. To capture the coexistence of inertial and creeping flows in the rock-ice mixtures, we use the Non-local Granular Fluidity (NGF) model (Henann & Kamrin, 2013), which bridges the two flow regimes through a scalar order-parameter-like fluidity field:

$$G = \dot{\gamma}/\mu \tag{6}$$

that is solved using the set of equations:

$$G = G^{\mathrm{in}} - \xi^2 \nabla^2 G \tag{7}$$

$$G^{\mathrm{in}} = H(\mu - \overline{\mu}_1)\sqrt{P/\overline{\rho}}\left(\overline{I}_o/\mu\overline{d}\right)\left[\frac{(\mu - \overline{\mu}_1)}{(\overline{\mu}_2 - \mu)}\right] \tag{8}$$

$$\xi = \lambda\overline{d}\sqrt{1/|\mu - \overline{\mu}_1|} \tag{9}$$

where $G^{\mathrm{in}} = \dot{\gamma}^{\mathrm{in}}(\mu^{\mathrm{in}}, P)/\mu$ in which $\dot{\gamma}^{\mathrm{in}}$ is obtained from the inertial rheology in Equation 1. When $\mu \leq \overline{\mu}_1$, the Heaviside function $H(\mu - \overline{\mu}_1)$ renders $G^{\mathrm{in}} = 0$, leaving only the Laplacian term to diffuse the fluidity over a characteristic length $\xi$ that depends on $\overline{d}$. The scalar magnitude $\lambda$ is the only free parameter in the model.

Equation 7 is solved computationally using the Python *solve_bvp* routine (Virtanen et al., 2020) while setting $G = 0$ at the base and $\partial G/\partial z = 0$ at the free-surface. The pressure is modeled as $P = \overline{\rho}\phi Hg\cos\theta$ where the volume fraction is assumed to be $\phi = 0.6$ for all cases. Once $G$ is obtained, $u$ can be calculated from Equation 6. Large and small particle distributions are obtained directly from DEM data. Figures 6b and 6c show that the calculated $G$ and $u/\sqrt{gH}$ profiles of the sample case agree well with the simulation results. Log-scale projections of the $x$-axis show that model and simulation deviate near the base since the NGF diffuses the mobility from the free surface and cannot capture the slight increase in shearing between the flowing and basal particle layers. We also obtain good agreement between modeled (lines) and simulated (symbols) $u/\sqrt{gH}$ profiles for flows in different segregation regimes and flowing angles (Figures 6d–6f) and for mixtures with $\mu_{ri}^{\mathrm{con}} = 0.05$ and $\mu_{ri}^{\mathrm{con}} = 0.1$ (Figures 6g–6i). See Table 1 for best-fit coefficients of single-phase gravity-driven flows having $\mu^{\mathrm{con}} = 0.05$ and $\mu^{\mathrm{con}} = 0.1$. Poor predictions for high angle cases are possibly due to the oversimplification of $\phi$ (which also varies with $I$) and the discrepancies observed between the contact probability model and data (see Figure 4b). Finally, we compare in Figure 6j the measured and modeled $u/\sqrt{gH}$ profiles for all gravity-driven flow simulations. Model accuracy is evaluated through the root-mean-square-logarithmic error (RMSLE) and the Thiel's measure of association ($T$) (see Appendix B for calculation

**Figure 6.** (a) Profile of a sample case $R = 0.7$, $\overline{C}_i = 0.5$, $\theta = 16°$ exhibiting heterogeneous flow. Inset shows that the $\mu$ in the creeping regions are non-local flows. Comparison between simulated (symbols) and theoretical (red lines) profiles of the (b) granular fluidity $G$ and (c) $u/\sqrt{gH}$ of the same sample case. (d) Simulated and modeled $u/\sqrt{gH}$ profiles of mixtures with (d) $R = 2$, (e) $R = 1$, and (f) $R = 0.5$ for a constant $\overline{C}_i = 0.5$ with different $\theta$. Modeled and measured velocity profiles when (g) $\mu_{ri}^{\mathrm{con}} = 0.01$, (g) $\mu_{ri}^{\mathrm{con}} = 0.05$, (g) $\mu_{ri}^{\mathrm{con}} = 0.1$. (j) Comparison between modeled and measured dimensionless $u$ for all test cases. The dashed line has a slope of 1.

details), which estimates the proximity of the data to the 1:1 line on a 0 to 1 scale (Lammers & Bledsoe, 2018). Both error metrics are low, showing good agreement of model and simulation despite spanning ∼4 orders of magnitude. We obtain the best simulation results using $\lambda = 0.4$ for all test cases.

## 4. Discussion

### 4.1. Implications for Rock-Ice Avalanche Modeling

We attempt to deepen our understanding of the micro-mechanisms relevant to rock-ice flow mobility using idealized DEM simulations. By discounting other complex factors such as fluidization by entrained fluids and meltwater (Mergili et al., 2020), acoustic fluidization (Collins & Melosh, 2003), fragmentation (Breard et al., 2023), flow over glaciers (De Blasio, 2014; Sosio et al., 2012) and cohesion (Ren et al., 2021) we highlight the role of interparticle friction and particle segregation through which useful observations and models are obtained. Rock-ice flows are simplified as isothermal, non-melting mixtures of rock and ice particles that segregate along the flow thickness due to differences in the particle size and density. Although steady-state segregation may not always be achieved in real rock-ice avalanches, this idealized scenario reveals that interparticle friction between rock and ice governs the mixture rheology. Segregation typically results in an ice-rich layer at the free-surface and a bottom rock-ice mixture region, separated by a sharp concentration gradient. Coupled with the large difference in the interparticle frictions of the rocks and ice, resulting from the frictional melting and very low surface friction of ice, segregation-induced mixture concentration results in strong feedbacks on the bulk flow dynamics. Flow layers largely composed of less frictional ice particles move faster because low interparticle friction lowers flow resistance. Since we set $\mu_{ri}^{\text{con}} = \mu_{ii}^{\text{con}}$, rock-rock contacts are the only highly frictional interactions in the system and are therefore the only type of contacts that can increase the flow resistance. Below the stopping angle of rocks, where pure rock mixtures are expected to be immobile, ice promotes flow by inducing low friction contacts. On the other hand, rock particles in ice-rich layers need to form a network of connections with each other to be able to diminish their mobility.

The rheology of dry rock-ice avalanches is intermediate to that of pure rock and ice flows (Schneider, Kaitna, et al., 2011). In the mechanistic rock-ice avalanche model of Pudasaini and Krautblatter (2014), which has been successfully used to model real rock-ice avalanches, the flow internal friction is calculated as a concentration-weighted sum of the rock and ice angles of repose. In comparison, here we find that the mixture internal friction is obtained from the weighted sum of single-phase rheologies, expressed through the $\mu^{\text{in}}(I)$ granular rheology, of flows with particle contact frictions similar to those of rocks on rocks, ice on ice, and rocks on ice. The weights are the probabilities that these contacts occur within the mixture, while the species concentration simply sets up these contact probabilities. In other words, the friction of rock-ice flows depends more on the distribution of frictional interactions than simply on the concentration of the rock and ice. The good agreement between the proposed mixture rheology and simulation data (Figure 6) shows that by accounting for the frictional contact probabilities, it is possible to model the inertial and non-local flow of rock-ice avalanches. The $\mu^{\text{in}}(I)$ rheology model is also well-accepted in simulating large-scale landslides (Moretti et al., 2012) and debris flows (Xie et al., 2022) and is now extended for two-species mixtures.

Although the dependence of the rheology on the interparticle frictional interactions are derived from idealized mixtures where $\mu_{ri}^{\text{con}} = \mu_{ii}^{\text{con}}$, the contact probability-weighted mixture rheology is generally applicable to mixtures where $\mu_{ii}^{\text{con}} \le \mu_{ri}^{\text{con}} < \mu_{rr}^{\text{con}}$ (see Figure 5b). The shear-rate dependent $\mu^{\text{in}}(I)$ granular rheology depends on three frictional coefficients—$\mu_1$, $\mu_2$, and $I_o$—which are obtained through data-fitting (Midi, 2004). These coefficients are not always readily known but can be calibrated from laboratory experiments of real rock and ice flows with real particle shapes and sizes, and numerical simulations (Midi, 2004). By applying the contact probabilities on these calibrated curves, it is possible to predict laboratory-scale and natural rock-ice avalanches.

Results here can also be applied to extra-terrestrial mass flows where ice is relevant. For instance, in Mars, $CO_2$ ice plays a crucial role in the formation of gullies (Roelofs et al., 2024). Ice sublimates due to the low Martian atmospheric pressures, which in turn fluidizes the flows. It is also hypothesized that external disturbances, such as marsquakes, rock falls, etc., trigger flows of sediment and $CO_2$ ice (Dundas et al., 2019). Heat loss due to this process further enhances the sublimation of $CO_2$ ice, which promotes transport over long distances. Aside from fluidization due to the sublimation of ice, it is also proposed that interactions with ice particles or frost-covered sediment (Hugenholtz, 2008) reduce friction at the contacts, contributing to the long run-out. Although particle segregation is not documented in such flows, the mixture rheology presented in this work may be useful in the modeling ice-laden mass flows in other planets.

### 4.2. Limitations

It is important to point out segregation scenarios that are not captured by our periodic flows but may be relevant in real rock-ice avalanches. Although all particles are assumed to be unbreakable, ice and rock can break down into smaller grains, especially in highly inertial flows, which means that segregation regimes may change as the flow progresses. In addition, the fragmentation of ice may speed up its melting. The fragmentation of both rock and ice will enhance the packing fraction of the flow, which in turn slows down the dissipation of excess pore water pressures, effectively fluidizing the flow (Breard et al., 2023). As a simplification necessary to study the segregation-mobility feedback in rock-ice avalanches, our simulations ignore saturation from excess meltwater generation and cohesion by liquid bridges at particle contacts. Both fluid effects are known to further diminish size segregation (Cui et al., 2021; Li & McCarthy, 2006) and may alter the segregation patterns observed in Figure 3. They may also contribute to the poor particle sorting in rock-ice avalanche deposits. Particle cohesion also fundamentally alters granular flow rheology (Vo et al., 2020) and the models used here may need to be re-defined to account for cohesive effects.

In geophysical flows, vertical segregation is typically a transient process which drives a particle species to the top before being preferentially transported to the front and sides (Baker et al., 2016; Kokelaar et al., 2014). The simulations here suggest that ice particles are more likely to be transported to the front and outer edges of the flow. This is consistent with experimental observations where ice tends to accumulate at the head of rapid rock-ice flows (C. Wang et al., 2022; Yang et al., 2019; Zhu et al., 2024), showing that vertical segregation inevitably occurs in rock-ice flows but is less obvious in real rock-ice avalanches, probably due to their much greater flowing thickness, melting of the ice particles, and presence of viscous interstitial pore fluids (Cui et al., 2021). On the other hand, the presence of pore fluids may further aid the segregation of ice particles due to buoyant effects. This also means that the vertical segregation presented here may not persist long enough to induce complex flow profiles that involve creeping. Nevertheless, the rheology presented here can still be applied to model the flow at different stages and degrees of segregation since the proposed weighting strategy is applicable for many mixture scenarios. Furthermore, the creeping flows that are observed here are idealized manifestations of non-local phenomena which are also relevant to real geophysical flows. Accounting for non-local effects improves flow modeling (S. Zhao et al., 2024) and the mixture composition dependent yield friction presented in this work can therefore be used to enhance three-dimensional geophysical flow models for rock-ice avalanches.

The complex flow profiles that result from segregation, involving both inertial and creeping flows, are modeled using a generalized non-local granular fluidity framework. Here, the best modeling results are obtained using a constant $\lambda = 0.4$. The free parameter $\lambda$ depends on the particle surface friction (Kamrin & Koval, 2014) and particle size (Henann & Kamrin, 2013). In rock-ice avalanches, these particle properties are mixed in varying proportions in different flow layers depending on the mixture conditions. To further generalize non-local flow models and improve the modeling results, it is important to better understand how the mixing of different particle properties influences granular fluidity. Model accuracy can also be improved by defining a volume fraction that accounts for the enhanced packing and dilatancy that results from mixing particles with different sizes (Tripathi & Khakhar, 2011) and surface roughness (Man et al., 2023). Effective sizes and densities are calculated through the concentration-weighted diameters and densities. Model accuracy is insensitive to whether mean sizes and densities are obtained for each flow layer or for the bulk mixture (see Figure S3 in Supporting Information S1). These mean quantities as well as the weighting model (Jiang et al., 2023) only account for the size ratios of two differently sized spherical particles (Figure 4b). Size distributions of rocks and ice in natural avalanches are wide and continuous and their shapes are angular and irregular. These two factors, may impact the mixture rheology by altering the contact probabilities. To improve its applicability to real rock-ice avalanches, the rheology model presented here should be extended to accommodate realistic particle shapes and size distributions.

## 5. Concluding Remarks

Using DEM simulations, we investigate the impacts of particle segregation, resulting from the size and density difference of rocks and ice, on the mobility of rock-ice avalanches. Rocks are simulated as highly frictional spherical particles, while ice is made less frictional to account for the lubrication by surface meltwater. Size and density segregation typically result in the upward rise of the ice particles to the free-surface, leaving a rock-rich mixture region near the base. Coupled with the large difference in the interparticle friction coefficients of the two particle species, segregation induces strong feedbacks to the bulk flow dynamics. Ice-rich flow layers flow faster as they experience lesser flow resistance resulting from low friction interactions, while flow layers that have more rock particles tend to move slower due to the increase in highly frictional interactions. In idealized segregation scenarios, rock-rich flow layers inclined below the stopping angle of rocks are nearly immobile driven to quasi-static flow only by the steady flowing ice-rich region. By promoting homogeneous particle layers, segregation induces complex flow velocity profiles involving both steady and creeping regimes.

The various segregation scenarios reveal that the mixture rheology of steady rock-ice flows is the weighted sum of the single-phase rheologies representing the frictional interactions between rocks on rocks, rocks on ice, and ice on ice. The weights are the probabilities of observing these frictional interactions within the mixture. The weighted mixture model captures the decrease in internal friction due to the presence of ice and predicts the transition in the yield conditions that separate inertial and creeping flows. The complex flow profiles are captured using a non-local granular fluidity framework modified to encode the dependence on the frictional contact probabilities. The results here provide fundamental insight into the role of frictional interactions, and their distribution within the mixture resulting from segregation on the mobility of rock-ice avalanches. This understanding is expected to enhance rock-ice avalanche models that are necessary for hazard mitigation and risk reduction.

## Appendix A: Governing Equation for the Discrete Element Method and Measurement of Bulk Kinematic Quantities From DEM

DEM simulations are conducted using the open-source code LIGGGHTS (Goniva et al., 2012), where particle interactions are solved using the Hertz contact model. In the DEM, the translational and rotational displacements of particles are calculated according to Newton's second law of motion:

$$m_a \frac{d^2 \boldsymbol{x_a}}{dt^2} = \sum_{b=1}^{N} \left(\boldsymbol{F}^c_{\text{norm}} + \boldsymbol{F}^c_{\tan}\right)_{ab} + m_a \boldsymbol{g} \tag{A1}$$

$$\boldsymbol{I_a} \frac{d\boldsymbol{\omega_a}}{dt} = \sum_{b=1}^{N} \boldsymbol{M}^c_{ab} \tag{A2}$$

for a single numerical time step. $m_a$ and $\boldsymbol{x_a}$ are the mass and position of a particle $a$, $N$ is the number of contacts. $\boldsymbol{F}^c_{\text{norm}}$ and $\boldsymbol{F}^c_{\tan}$ are the normal and tangential forces, calculated using the Hertz model, defined at a contact point $c$. $\boldsymbol{I_a}$ is the moment of inertia of a sphere, $\boldsymbol{\omega_a}$ is the particles' rotational acceleration and $\boldsymbol{M}^c_{ab}$ is the moment exerted by a particle $b$ on $a$.

Kinematic and rheological properties were calculated for each sampling volume $V_M = L \times W \times 2d_S$. The volume fraction $\phi$ and streamwise velocity $u$ belonging to a single particle species $k = i, r$ are calculated as

$$\phi_k = \frac{\sum_a V_{a,k}}{V_M} \tag{A3}$$

$$u_k = \frac{\sum_a u_{a,k} V_{a,k}}{\sum_a V_{a,k}} \tag{A4}$$

respectively. $V_{a,k}$ is the portion of a sphere $a$ that falls within the sampling volume. The shear rate is calculated as $\dot{\gamma} = \left| du/_{dz} \right|$ where $u = \sum_k u_k$. The total stress tensor is the sum of the kinetic and contact components. The partial kinetic stress tensor of a particle species within $V_M$ is calculated as

$$\boldsymbol{\sigma}_k^{\text{kin}} = \frac{1}{V_M} \sum_a m_{a,k} \boldsymbol{\Lambda}_{a,k} \otimes \boldsymbol{\Lambda}_{a,k} \tag{A5}$$

where $\boldsymbol{\Lambda}_{a,k}$ is the fluctuating velocity defined as the difference between the instantaneous and time-averaged velocities. The contact stress tensor is calculated as

$$\boldsymbol{\sigma}_k^{\text{con}} = \frac{1}{V_M} \left[ \sum_{a \neq b} \boldsymbol{F}_{ab,k} \otimes \boldsymbol{R}_{ab,k} \right] \tag{A6}$$

where $\boldsymbol{F}_{ab} = \boldsymbol{F}_{\text{norm}}^c + \boldsymbol{F}_{\text{tan}}^c$ is the contact force between particles $a$ and $b$ where $a$ belongs to the species $k$. $\boldsymbol{R}_{ab}$ is the distance between their centers. The total stress is computed as:

$$\boldsymbol{\sigma_k} = \boldsymbol{\sigma}_k^{\text{Kin}} + \boldsymbol{\sigma}_k^{\text{Con}} \tag{A7}$$

The total mixture pressure is $\boldsymbol{\sigma} = \sum_k \boldsymbol{\sigma_k}$ from which the pressure $P = \boldsymbol{\sigma_{zz}}$ and shear stress $\tau = \boldsymbol{\sigma_{xz}}$ are obtained.

## Appendix B: Quantifying Prediction Accuracy

Overall prediction accuracy between model velocity predictions $u_{\text{pred},j}$ and DEM results $u_j$ per flowing layer $j$ of which there $n$, are quantified by the root-mean-square-logarithmic error (RMSLE):

$$\text{RMSLE} = \sqrt{\frac{1}{n} \sum_{j=1}^{n} \left( \log u_j - \log u_{\text{pred},j} \right)^2} \tag{B1}$$

and the Thiel's measure of association:

$$T = \frac{\sqrt{\frac{1}{n} \sum_{j=1}^{n} \left( u_j - u_{\text{pred},j} \right)^2}}{\sqrt{\frac{1}{n} \sum_{j=1}^{n} \left( u_j \right)^2} + \sqrt{\frac{1}{n} \sum_{j=1}^{n} \left( u_{\text{pred},j} \right)^2}} \tag{B2}$$

## Conflict of Interest

The authors declare no conflicts of interest relevant to this study.

## Data Availability Statement

Data and codes that can be used to replicate and validate the results presented here are available at Cui et al. (2024).

**Acknowledgments**
The authors acknowledge the financial support from the National Key R&D Program of China (No. 2023YFC3008300, 2023YFC3008302), National Natural Science Foundation of China (Grant 12250410257), the Science and Technology Research Program of Institute of Mountain Hazards and Environment, Chinese Academy of Sciences (No. IMHE-ZDRW-03), and Key Collaborative Research Program of the Alliance of International Science Organizations (Grant ANSO-CR-KP-2021-07), and Sichuan Science and Technology Program (2024NSFJQ0043). We are grateful to Olga Sergienko, Katy Barnhart, and three anonymous reviewers for their detailed and constructive comments on the manuscript.

## References

Baker, J., Gray, J. M. N. T., & Kokelaar, B. P. (2016). Particle size-segregation and spontaneous levee formation in geophysical granular flows. *International Journal of Erosion*, *9*(4), 174–178. https://doi.org/10.13101/ijece.9.174

Barker, T., Rauter, M., Maguire, E. S. F., Johnson, C. G., & Gray, J. M. N. T. (2021). Coupling rheology and segregation in granular flows. *Journal of Fluid Mechanics*, *909*, A22. https://doi.org/10.1017/jfm.2020.973

Breard, E. C. P., Dufek, J., Charbonnier, S., Gueugneau, V., Giachetti, T., & Walsh, B. (2023). The fragmentation-induced fluidisation of pyroclastic density currents. *Nature Communications*, *14*(1), 2079. https://doi.org/10.1038/s41467-023-37867-1

Collins, G. S., & Melosh, H. J. (2003). Acoustic fluidization and the extraordinary mobility of sturzstroms. *Journal of Geophysical Research*, *108*(B10), 1–14. https://doi.org/10.1029/2003jb002465

Cui, K. F. E., Zhou, G., Jing, L., Mangeney, A., Cui, Y., Huang, Y., & Chen, X. (2024). Data for “Segregation-induced flow transitions in rock-ice avalanches” [Dataset]. *Zenodo*. https://doi.org/10.5281/zenodo.13500791

Cui, K. F. E., Zhou, G. G. D., & Jing, L. (2021). Viscous effects on the particle size segregation in geophysical mass flows: Insights from immersed granular shear flow simulations. *Journal of Geophysical Research: Solid Earth*, *126*(8), 1–21. https://doi.org/10.1029/2021jb022274

De Blasio, F. V. (2014). Friction and dynamics of rock avalanches travelling on glaciers. *Geomorphology*, *213*, 88–98. https://doi.org/10.1016/j.geomorph.2014.01.001

Delannay, R., Valance, A., Mangeney, A., Roche, O., & Richard, P. (2017). Granular and particle-laden flows: From laboratory experiments to field observations. *Journal of Physics D: Applied Physics*, *50*(5), 53001. https://doi.org/10.1088/1361-6463/50/5/053001

Deline, P., Gruber, S., Amann, F., Bodin, X., Delaloye, R., Failletaz, J., et al. (2021). Ice loss from glaciers and permafrost and related slope instability in high-mountain regions. In *Snow and ice-related hazards, risks, and disasters*. https://doi.org/10.1016/b978-0-12-817129-5.00015-9

Deline, P., Hewitt, K., Reznichenko, N., & Shugar, D. H. (2014). Rock avalanches onto glaciers. In *Landslide hazards, risks, and disasters*. https://doi.org/10.1016/B978-0-12-396452-6.00009-4

Dong, Z. B., & Su, L. (2024). Flow regimes and basal normal stresses in rock–ice avalanches by experimental rotating drum tests. *Cold Regions Science and Technology*, *218*, 104081. https://doi.org/10.1016/j.coldregions.2023.104081

Duan, Y., Umbanhowar, P. B., Ottino, J. M., & Lueptow, R. M. (2021). Modelling segregation of bidisperse granular mixtures varying simultaneously in size and density for free surface flows. *Journal of Fluid Mechanics*, *918*, 1–32. https://doi.org/10.1017/jfm.2021.342

Dundas, C. M., McEwen, A. S., Diniega, S., Hansen, C. J., Byrne, S., & McElwaine, J. N. (2019). The formation of gullies on Mars today. *Geological Society - Special Publications*, *467*(1), 67–94. https://doi.org/10.1144/SP467.5

Evans, S. G., Bishop, N. F., Fidel, L., Valderrama, P., Delaney, K. B., & Oliver-smith, A. (2009). A re-examination of the mechanism and human impact of catastrophic mass flows originating on Nevado Huascarán, Cordillera Blanca, Peru in 1962 and 1970. *Engineering Geology*, *108*(1–2), 96–118. https://doi.org/10.1016/j.enggeo.2009.06.020

Evans, S. G., Tutubalina, O., Drobyshev, V. N., Chernomorets, S., McDougall, S., Petrakov, D. A., & Hungr, O. (2009). Catastrophic detachment and high-velocity long-runout flow of Kolka Glacier, Caucasus Mountains, Russia in 2002. *Geomorphology*, *105*(3–4), 314–321. https://doi.org/10.1016/j.geomorph.2008.10.008

Favreau, P., Mangeney, A., Lucas, A., Crosta, G., & Bouchut, F. (2010). Numerical modeling of landquakes. *Geophysical Research Letters*, *37*(15), 1–5. https://doi.org/10.1029/2010GL043512

Feng, Z., Fan, X., Ni, T., Deng, Y., Zou, C., Zhang, J., & Xu, Q. (2023). How ice particles increase mobility of rock-ice avalanches: Insights from chute flows simulation of granular rock-ice mixtures by discrete element method. *Journal of Geophysical Research: Earth Surface*, *128*(8), e2023JF007115. https://doi.org/10.1029/2023JF007115

Fry, A. M., Umbanhowar, P. B., Ottino, J. M., & Lueptow, R. M. (2018). Effect of pressure on segregation in granular shear flows. *Physical Review*, *97*(6), 1–10. https://doi.org/10.1103/PhysRevE.97.062906

Gammon, B. P. H., Kiefte, H., Clouter, M. J., & Dennert, W. W. (1983). Elastic constants of artificial and natural ice. *Journal of Glaciology*, *29*(103), 433–460. https://doi.org/10.1017/s0022143000030355

Gnyawali, K. R., Xing, A., & Zhuang, Y. (2020). Dynamic analysis of the multi-staged ice—Rock debris avalanche in the Langtang valley triggered by the 2015 Gorkha earthquake, Nepal. *Engineering Geology*, *265*, 105440. https://doi.org/10.1016/j.enggeo.2019.105440

Gold, L. W. (1977). Engineering properties of fresh water ice. *Journal of Glaciology*, *19*(81), 197–212. https://doi.org/10.3189/s0022143000215608

Goniva, C., Kloss, C., Deen, N. G., Kuipers, J. A. M., & Pirker, S. (2012). Influence of rolling friction on single spout fluidized bed simulation. *Particuology*, *10*(5), 582–591. https://doi.org/10.1016/j.partic.2012.05.002

Gray, J. M. N. T. (2018). Particle segregation in dense granular flows. *Annual Review of Fluid Mechanics*, *50*(1), 407–433. https://doi.org/10.1146/annurev-fluid-122316

Gray, J. M. N. T., & Ancey, C. (2015). Particle-size and -density segregation in granular free-surface flows. *Journal of Fluid Mechanics*, *779*, 622–668. https://doi.org/10.1017/jfm.2015.438

Haeberli, W., Huggel, C., Ka, A., Zgraggen-oswald, S., Polkvoj, A., Galushkin, I., et al. (2015). The Kolka-Karmadon rock/ice slide of 20 September 2002: An extraordinary event of historical dimensions in North Ossetia, Russian Caucasus. *Journal of Glaciology*, *50*(171). https://doi.org/10.3189/172756504781829710

Henann, D. L., & Kamrin, K. (2013). A predictive, size-dependent continuum model for dense granular flows. *Proceedings of the National Academy of Sciences of the United States of America*, *110*(17), 6730–6735. https://doi.org/10.1073/pnas.1219153110

Higa, M., Arakawa, M., & Maeno, N. (1996). Measurements of restitution coefficients of ice at low temperatures. *Planetary and Space Science*, *44*(9), 917–925. https://doi.org/10.1016/0032-0633(95)00133-6

Hugenholtz, C. H. (2008). Frosted granular flow: A new hypothesis for mass wasting in Martian gullies. *Icarus*, *197*(1), 65–72. https://doi.org/10.1016/j.icarus.2008.04.010

Huggel, C., Salzmann, N., Allen, S., Fischer, L., Haeberli, W., Schneider, D., & Wessels, R. (2010). Recent and future warm extreme events and high-mountain slope stability. *Philosophical Transactions of the Royal Society A: Mathematical, Physical & Engineering Sciences*, *368*(1919), 2435–2459. https://doi.org/10.1098/rsta.2010.0078

Jiang, H., Jiang, X., & Matsushima, T. (2023). Rheology of segregated bidisperse granular flow in an inclined plane. *Journal of Japan Society of Civil Engineers, Ser. A2 (Applied Mechanics (AM))*, *11*(2). https://doi.org/10.2208/journalofjsce.22-15035

Jing, L., Kwok, C. Y., & Leung, Y. F. (2017). Micromechanical origin of particle size segregation. *Physical Review Letters*, *118*(11), 118001. https://doi.org/10.1103/PhysRevLett.118.118001

Jing, L., Ottino, J. M., Lueptow, R. M., & Umbanhowar, P. B. (2020). Rising and sinking intruders in dense granular flows. *Physical Review Research*, *2*(2), 22069. https://doi.org/10.1103/PhysRevResearch.2.022069

Jones, S., Kitagawa, H., Izumiyama, K., & Shimoda, H. (1994). Friction of melting ice. *Annals of Glaciology*, *19*, 7–12. https://doi.org/10.3189/1994aog19-1-7-12

Jop, P., Forterre, Y., & Pouliquen, O. (2006). A constitutive law for dense granular flows. *Nature*, *441*(7094), 727–730. https://doi.org/10.1038/nature04801

Kääb, A., Jacquemart, M., Gilbert, A., Leinss, S., Girod, L., Huggel, C., et al. (2021). Sudden large-volume detachments of low-angle mountain glaciers – More frequent than thought. *The Cryosphere*, *15*(4), 1751–1785. https://doi.org/10.5194/tc-15-1751-2021

Kamrin, K., & Koval, G. (2014). Effect of particle surface friction on nonlocal constitutive behavior of flowing granular media. *Computational Particle Mechanics*, *1*(2), 169–176. https://doi.org/10.1007/s40571-014-0018-3

Kokelaar, B. P., Graham, R. L., Gray, J. M. N. T., & Vallance, J. W. (2014). Fine-grained linings of leveed channels facilitate runout of granular flows. *Earth and Planetary Science Letters*, *385*, 172–180. https://doi.org/10.1016/j.epsl.2013.10.043

Lammers, R. W., & Bledsoe, B. P. (2018). Parsimonious sediment transport equations based on Bagnold's stream power approach. *Earth Surface Processes and Landforms*, *43*(1), 242–258. https://doi.org/10.1002/esp.4237

Li, H., & McCarthy, J. J. (2006). Cohesive particle mixing and segregation under shear. *Powder Technology*, *164*(1), 58–64. https://doi.org/10.1016/j.powtec.2005.12.018

Man, T., Zhang, P., Ge, Z., Galindo-Torres, S. A., & Hill, K. M. (2023). Friction-dependent rheology of dry granular systems. *Acta Mechanica Sinica*, *39*(1), 1–11. https://doi.org/10.1007/s10409-022-22191-x

Man, T., Zhang, Z., Huppert, H. E., & Galindo-Torres, S. A. (2022). Axisymmetric column collapses of bi-frictional granular mixtures. *Journal of Fluid Mechanics*, *963*, A4. https://doi.org/10.1017/jfm.2023.217

Mergili, M., Jaboyedoff, M., Pullarello, J., & Pudasaini, S. P. (2020). Back calculation of the 2017 Piz Cengalo—Bondo landslide cascade with r.avaflow: What we can do and what we can learn. *Natural Hazards and Earth System Sciences*, *20*(2), 505–520. https://doi.org/10.5194/nhess-20-505-2020

Midi, G. D. R. (2004). On dense granular flows. *European Physical Journal E*, *14*(4), 341–365. https://doi.org/10.1140/epje/i2003-10153-0

Moretti, L., Allstadt, K., Mangeney, A., Capdeville, Y., Stutzmann, E., & Bouchut, F. (2015). Numerical modeling of the Mount Meager landslide constrained by its force history derived. *Journal of Geophysical Research: Solid Earth*, *120*(4), 2579–2599. https://doi.org/10.1002/2014JB011426.Received

Moretti, L., Mangeney, A., Capdeville, Y., Stutzmann, E., Huggel, C., Schneider, D., & Bouchut, F. (2012). Numerical modeling of the Mount Steller landslide flow history and of the generated long period seismic waves. *Geophysical Research Letters*, *39*(L16402), 1–7. https://doi.org/10.1029/2012GL052511

Noetzli, J., Huggel, C., Hoelzle, M., & Haeberli, W. (2006). GIS-based modelling of rock-ice avalanches from Alpine permafrost areas. *Computational Geosciences*, *10*(2), 161–178. https://doi.org/10.1007/s10596-005-9017-z

Pouliquen, O. (1999). Scaling laws in granular flows down rough inclined planes. *Physics of Fluids*, *11*(1999), 542–548. https://doi.org/10.1063/1.869928

Pouragha, M., Jebeli, M., & Glade, R. (2023). Failure of partially saturated frozen soils: A micromechanical analysis. *Cold Regions Science and Technology*, *210*, 1–12. https://doi.org/10.1016/j.coldregions.2023.103842

Pudasaini, S. P., & Krautblatter, M. (2014). A two-phase mechanical model for rock-ice avalanches. *Journal of Geophysical Research: Earth Surface*, *119*(10), 2272–2290. https://doi.org/10.1002/2014JF003183

Ren, Y., Yang, Q., Cheng, Q., Cai, F., & Su, Z. (2021). Solid-liquid interaction caused by minor wetting in gravel-ice mixtures: A key factor for the mobility of rock-ice avalanches. *Engineering Geology*, *286*, 106072. https://doi.org/10.1016/j.enggeo.2021.106072

Roelofs, L., Conway, S. J., van Dam, B., van Eijk, A., Merrison, J. P., Iversen, J. J., et al. (2024). The dynamics of $CO_2$-driven granular flows in gullies on Mars. *Journal of Geophysical Research: Planets*, *129*(6), 1–13. https://doi.org/10.1029/2024JE008319

Sansone, S., Zugliani, D., & Rosatti, G. (2021). A mathematical framework for modelling rock-ice avalanches. *Journal of Fluid Mechanics*, *919*, 1–53. https://doi.org/10.1017/jfm.2021.348

Schneider, D., Huggel, C., Haeberli, W., & Kaitna, R. (2011). Unraveling driving factors for large rock-ice avalanche mobility. *Earth Surface Processes and Landforms*, *36*(14), 1948–1966. https://doi.org/10.1002/esp.2218

Schneider, D., Kaitna, R., Dietrich, W. E., Hsu, L., Huggel, C., & McArdell, B. W. (2011). Frictional behavior of granular gravel-ice mixtures in vertically rotating drum experiments and implications for rock-ice avalanches. *Cold Regions Science and Technology*, *69*(1), 70–90. https://doi.org/10.1016/j.coldregions.2011.07.001

Shen, W., Zhao, T., Dai, F., Crosta, G. B., & Wei, H. (2020). Discrete element Analyses of a realistic-shaped rock block impacting against a Soil Buffering layer. In *Rock mechanics and rock engineering*. https://doi.org/10.1007/s00603-020-02116-0

Shugar, D. H., Jacquemart, M., Shean, D., Bhushan, S., Upadhyay, K., Sattar, A., et al. (2021). A massive rock and ice avalanche caused the 2021 disaster at Chamoli, Indian Himalaya. *Science*, *373*, 300–306. https://doi.org/10.1126/science.abh4455

Silbert, L. E., Ertas, D., Grest, G. S., Halsey, T. C., Levine, D., & Plimpton, S. J. (2001). Granular flow down an inclined plane: Bagnold scaling and rheology. *Physical Review*, *64*(051302), 1–14. https://doi.org/10.1103/PhysRevE.64.051302

Sosio, R. (2015). Rock-snow-ice avalanches. In *Landslide hazards, risks, and disasters*. https://doi.org/10.1016/B978-0-12-396452-6.00007-0

Sosio, R., Crosta, G. B., Chen, J. H., & Hungr, O. (2012). Modelling rock avalanche propagation onto glaciers. *Quaternary Science Reviews*, *47*, 23–40. https://doi.org/10.1016/j.quascirev.2012.05.010

Tripathi, A., & Khakhar, D. V. (2011). Rheology of binary granular mixtures in the dense flow regime. *Physics of Fluids*, *23*(11). https://doi.org/10.1063/1.3653276

Tunuguntla, D. R., Bokhove, O., & Thornton, A. R. (2014). A mixture theory for size and density segregation in shallow granular free-surface flows. *Journal of Fluid Mechanics*, *749*(2014), 99–112. https://doi.org/10.1017/jfm.2014.223

Turnbull, B. (2011). Scaling laws for melting ice avalanches. *Physical Review Letters*, *107*(25), 258001. https://doi.org/10.1103/PhysRevLett.107.258001

Virtanen, P., Gommers, R., Oliphant, T. E., Haberland, M., Reddy, T., Cournapeau, D., et al. (2020). SciPy 1.0: Fundamental algorithms for scientific computing in Python. *Nature Methods*, *17*(3), 261–272. https://doi.org/10.1038/s41592-019-0686-2

Vo, T. T., Nezamabadi, S., Mutabaruka, P., Delenne, J. Y., & Radjai, F. (2020). Additive rheology of complex granular flows. *Nature Communications*, *11*(1), 1–8. https://doi.org/10.1038/s41467-020-15263-3

Wang, C., Cui, Y., Song, D., Nie, J., & Hu, B. (2022). Effect of ice content on the interaction between rock–ice avalanche and rigid barrier: Physical and numerical modelling. *Computers and Geotechnics*, *150*, 104924. https://doi.org/10.1016/j.compgeo.2022.104924

Wang, G., & Calvetti, F. (2021). 3D DEM investigation of the resistance of ice and frozen granular soils. *European Journal of Environmental and Civil Engineering*, 1–21. https://doi.org/10.1080/19648189.2021.2021997

Xie, Y., Zhou, G. G. D., Cui, K. F. E., & Lu, X. (2022). Numerical investigation of debris flows using a two-phase continuum model incorporating a visco-inertial rheology. *Engineering Geology*, *308*, 106797. https://doi.org/10.1016/j.enggeo.2022.106797

Yang, Q., Su, Z., Cheng, Q., Ren, Y., & Cai, F. (2019). High mobility of rock-ice avalanches: Insights from small flume tests of gravel-ice mixtures. *Engineering Geology*, *260*, 105260. https://doi.org/10.1016/j.enggeo.2019.105260

Zhao, S., He, S., Li, X., Scaringi, G., Liu, Y., & Deng, Y. (2024). Investigating the dynamic process of a rock avalanche through an MLS-MPM simulation incorporated with a nonlocal μ(I) rheology model. *Landslides*, *21*, 1483–1499. https://doi.org/10.1007/s10346-024-02244-6

Zhao, T., & Liu, Y. (2020). A novel random discrete element analysis of rock fragmentation. *International Journal for Numerical and Analytical Methods in Geomechanics*, *44*(10), 1386–1395. https://doi.org/10.1002/nag.3067

Zhu, Y., Jiang, Y., Liu, Y., Xie, Q., Hu, X., & Xia, X. (2024). Material characteristic-controlled particle segregation in rock-ice avalanche. *Computers and Geotechnics*, *171*, 106367. https://doi.org/10.1016/j.compgeo.2024.106367

## Erratum

The originally published version of this article contained a typographical error in the Acknowledgments. The grant number 2023YFC300830 of the funding agency the National Key R&D Program of China should be 2023YFC3008300. The error has been corrected, and this may be considered the authoritative version of record.